

NOTICE: This is the accepted author manuscript of the publication

Decreased in vivo availability of the cannabinoid type 2 receptor in Alzheimer's disease.

Ahmad R, Postnov A, Bormans G, Versijpt J, Vandenbulcke M, Van Laere K.

Published in European Journal of Nuclear Medicine and Molecular Imaging

November 2016, Volume 43, Issue 12, pp 2219–2227

doi: 10.1007/s00259-016-3457-7

Available online 3 August 2016

Direct link to the final version of the article:

<https://doi.org/10.1007/s00259-016-3457-7>

<https://link.springer.com/article/10.1007%2Fs00259-016-3457-7>

© <2017>. This manuscript version is made available under the CC-BY-NC-ND 4.0 license
<http://creativecommons.org/licenses/by-nc-nd/4.0/>

European Journal of Nuclear Medicine and Molecular Imaging

Decreased in vivo availability of the cannabinoid type 2 receptor in Alzheimer's disease


--Manuscript Draft--

Manuscript Number:	EJNM-D-16-00117R1
Full Title:	Decreased in vivo availability of the cannabinoid type 2 receptor in Alzheimer's disease
Article Type:	Original Article
Corresponding Author:	Rawaha Ahmad, M.D. Department of Imaging and Pathology, Nuclear Medicine and Molecular Imaging, KU Leuven and University Hospitals Leuven Leuven, Vlaams Brabant BELGIUM
Corresponding Author Secondary Information:	
Corresponding Author's Institution:	Department of Imaging and Pathology, Nuclear Medicine and Molecular Imaging, KU Leuven and University Hospitals Leuven
Corresponding Author's Secondary Institution:	
First Author:	Rawaha Ahmad, M.D.
First Author Secondary Information:	
Order of Authors:	Rawaha Ahmad, M.D. Andrey Postnov Guy Bormans Jan Versijpt Mathieu Vandenbulcke Koen Van Laere
Order of Authors Secondary Information:	
Funding Information:	
Abstract:	<p>Purpose : The cannabinoid type 2 receptor (CB2R) is expressed by immune cells such as monocytes and macrophages. In the brain, CB2R is primarily found on microglia. CB2R upregulation has been reported in animal models of Alzheimer's disease, with a preferential localization near amyloid beta (Aβ) plaques and post-mortem patients. Here, we have performed in vivo brain imaging and kinetic modeling of the CB2R tracer [11C]-NE40 in healthy controls (HC) and in patients with Alzheimer's disease (AD), to investigate whether an in vivo increase in CB2R availability is present, regionally colocalized to amyloid beta deposits.</p> <p>Methods : Dynamic 90 minute [11C]-NE40 PET scans were performed on 8 HC and 9 AD patients with full kinetic modeling using arterial sampling and metabolite correction and partial volume correction. All AD patients received a static [11C]-PIB scan 40 minutes after injection. In 4 HC, a retest scan with [11C]-NE40 PET was performed within 9 weeks to investigate test-retest characteristics.</p> <p>Results : [11C]-NE40 was metabolized quickly leading to 50% of intact tracer 20 minutes post injection (PI) and 20% at 90 minutes PI. A two-tissue (2T) kinetic model fitted most of the time activity curves (TAC) best; both binding potential (BPND) and distribution volume (VT) parameters could be used. Brain uptake was generally low with an average K1 value of 0.07 ml/min/ml tissue. VT and BPND were in the range of 0.7-1.8 and 0.6-1.6 respectively. Test- values in HC were about 30% for VT and BPND. AD patients showed an overall significant decrease of CB2R binding. No relationship was found between regional or global amyloid load and CB2R availability.</p> <p>Conclusions : Kinetic modeling of [11C]-NE40 is possible with a 2T reversible model. In contrast to preclinical and post-mortem data, [11C]-NE40 PET shows an in vivo decrease of CB2R availability in AD patients, without a relationship to amyloid beta plaques. A possible explanation for these findings is a too low CB2R binding affinity</p>

[Click here to view linked References](#)1
2
3
4
5
6
7
8
9
10
11
12
13
14
15
16
17
18
19
20
21
22
23
24
25
26
27
28
29
30
31
32
33
34
35
36
37
38
39
40
41
42
43
44
45
46
47
48
49
50
51
52
53
54
55
56
57
58
59
60
61
62
63
64
65

1

Decreased in vivo availability of the cannabinoid type 2 receptor in Alzheimer's disease

Rawaha Ahmad^{1*}, Andrey Postnov^{1*}, Guy Bormans², Jan Versijpt , Mathieu
~~Vandenbuleke³~~Vandenbulcke⁴, Koen Van Laere¹

Commented [KL1]: have changed the number as occurring in the list.

1. Department of Imaging & Pathology, Nuclear Medicine and Molecular Imaging, KU Leuven and University Hospitals Leuven, Leuven, Belgium
2. Laboratory for Radiopharmacy, KU Leuven, Belgium
3. ~~Old Age Psychiatry, Department of Psychiatry, KU Leuven and University Hospitals Leuven, Leuven, Belgium~~
4. Department of Neurology, University Hospital Brussels, Brussels, Belgium
5. Old Age Psychiatry, Department of Psychiatry, KU Leuven and University Hospitals Leuven, Leuven, Belgium

Corresponding author:

Dr. Rawaha Ahmad
Division of Nuclear Medicine
University Hospital Leuven, Herestraat 49
E901
3000 Leuven, Belgium
Tel. +32-16-343715, Fax +32-16-343759.
E-mail: Rawaha.ahmad@uzleuven.be

* both authors contributed equally

1
2
3
4
5
6
7
8
9
10
11
12
13
14
15
16
17
18
19
20
21
22
23
24
25
26
27
28
29
30
31
32
33
34
35
36
37
38
39
40
41
42
43
44
45
46
47
48
49
50
51
52
53
54
55
56
57
58
59
60
61
62
63
64
65

Acknowledgements

The authors thank prof. dr. Wim Vandenberghe for revising the manuscript content. We also thank Mr. Kwinten Porters, Mrs. Mieke Steukers and Ms. Hannelore Bels as well as the clinical PET radiopharmacy team (especially Mrs. Marva Bex and dr. pharm. Kim Serdons) for their contributions in the execution of the study. KVL is Senior Research Fellow for the Flemish Scientific Research Foundation, Belgium (FWO Vlaanderen). [This research was partially sponsored by EU FP7 Grant FP7/2007-2013, INMiND, grant agreement no. 278850.](#)

Formatted: Dutch (Belgium)

Formatted: Font: (Default) Times New Roman, 12 pt, Dutch (Belgium)

Formatted: Font: (Default) Times New Roman

Abstract

Purpose : The cannabinoid type 2 receptor (CB₂R) is expressed by immune cells such as monocytes and macrophages. In the brain, CB₂R is primarily found on microglia. CB₂R upregulation has been reported in animal models of Alzheimer's disease, with a preferential localization near amyloid beta (A β) plaques and post-mortem patients. Here, we have performed in vivo brain imaging and kinetic modeling of the CB₂R tracer [¹¹C]-NE40 in healthy controls (HC) and in patients with Alzheimer's disease (AD), to investigate whether an in vivo increase in CB₂R availability is present, regionally colocalized to amyloid beta deposits.

Methods : Dynamic 90 minute [¹¹C]-NE40 PET scans were performed on 8 HC and 9 AD patients with full kinetic modeling using arterial sampling and metabolite correction and partial volume correction. All AD patients received a static [¹¹C]-PIB scan 40 minutes after injection. In 4 HC, a retest scan with [¹¹C]-NE40 PET was performed within 9 weeks to investigate test-retest characteristics.

Results : [¹¹C]-NE40 was metabolized quickly leading to 50% of intact tracer 20 minutes post injection (PI) and 20% at 90 minutes PI. A two-tissue (2T) kinetic model fitted most of the time activity curves (TAC) best; both binding potential (BP_{ND}) and distribution volume (V_T) parameters could be used. Brain uptake was generally low with an average K₁ value of 0.07 ml/min/ml tissue. V_T and BP_{ND} were in the range of 0.7-1.8 and 0.6-1.6 respectively. Test- values in HC were about 30% for V_T and BP_{ND}. AD patients showed an overall significant decrease of CB₂R binding. No relationship was found between regional or global amyloid load and CB₂R availability.

Conclusions : Kinetic modeling of [¹¹C]-NE40 is possible with a 2T reversible model. In contrast to preclinical and post-mortem data, [¹¹C]-NE40 PET shows an in vivo decrease of CB₂R availability in AD patients, without a relationship to amyloid beta plaques. [A -possible](#)

1
2
3
4
5
6
7
8
9
10
11
12
13
14
15
16
17
18
19
20
21
22
23
24
25
26
27
28
29
30
31
32
33
34
35
36
37
38
39
40
41
42
43
44
45
46
47
48
49
50
51
52
53
54
55
56
57
58
59
60
61
62
63
64
65

explanation for these findings- is a the too low CB2R insufficient CB2R-binding affinity and/or selectivity versus CB1R of [¹¹C]-NE40 the radiotracer.

Keywords:

Cannabinoid type 2 receptor – CB₂R - neuroinflammation – PET imaging – Alzheimer’s disease.

Introduction

Most neurodegenerative disorders, including Alzheimer’s disease (AD), are proteinopathies that are associated with the aggregation and accumulation of misfolded proteins [1]. Aggregated proteins are potent activators of an immune response in the brain leading to neuroinflammation [2]. In this process, microglia become activated and upregulate an array of receptors that may be critical in microglial regeneration and/or degeneration of the central nervous system (CNS) [3]. Among these are the mitochondrial membrane 18kDa translocator protein (TSPO), the type 2 cannabinoid receptor (CB₂R), the P₂X₇ receptor and matrix metalloproteinases (MMPs) [4]. The TSPO target has been extensively studied using PET imaging approaches over the past decades. [¹¹C]-PK11195 showed cortical upregulation of TSPO in different brain regions in AD [5, 6]. To resolve the high non-specific binding, low signal-to-background ratio and cumbersome quantification of [¹¹C]-PK11195, several new TSPO radioligands were developed, such as [¹⁸F]DPA-714, [¹⁸F]FEDAA1106, [¹⁸F]-FEPPA, and [¹¹C]-PBR28 (for overview see [4]). The CB₂R is an alternative membrane marker of activated microglial cells and it forms part of the endogenous cannabinoid system (ECS), together with type 1 cannabinoid receptor (CB₁R), their endogenous ligands (endocannabinoids), their transport and degrading enzymes.

Field Code Changed

Field Code Changed

Field Code Changed

Field Code Changed

Field Code Changed

Field Code Changed

Field Code Changed

Upon microglial activation, CB₂R expression is also markedly elevated [7]. Studies in small animal models and post-mortem studies in patients have shown an upregulation of CB₂R in various CNS disorders that are accompanied with neuroinflammation. A recent study showed CB₂R activation in a bigenic mouse model of AD with A β amyloidosis without concomitant tau pathology [8]. Immunofluorescent analysis showed that CB₂R expression in activated microglia was the main source for the differential PET signal, while neuronal CB₂R density was unchanged [8]. Also, in post-mortem brain tissue of AD patients, CB₂R was selectively upregulated in neuritic plaque-associated glia [9]. In a Huntington's disease (HD) transgenic mouse model [10], microglial CB₂R had a neuroprotective role, and in animal models of Parkinson's disease (PD), pharmacological agonism of CB₂R was also protective against nigrostriatal cell loss [11].

Therefore, CB₂R PET imaging may provide a novel type of biomarker for neurodegeneration-associated neuroinflammation and could be a valuable tool to guide specific CB₂R-related therapeutic interventions. A number of PET radiotracers for CB₂R have been published recently [12-14], but so far no human brain CB₂R PET studies have been published. Our group has developed the CB₂R tracer 2-oxo-7-[¹¹C]-methoxy-8butyloxy-1,2-dihydroquinoline-3-carboxylic acid ([¹¹C]-NE40), which has favourable affinity (K_i=9.6 nM for CB₂R) and kinetics for CNS imaging [15]. It was validated preclinically in animal models with local overexpression of human CB₂R [16]. The aims of the current study were to evaluate full brain kinetic modeling of [¹¹C]-NE40 and to investigate the hypothesis that an in vivo increased CB₂R availability is present in AD brain, colocalized at sites of amyloid-beta deposition.

Materials and methods

Subjects

Healthy controls (HC) (male and female, age > 40 years) were recruited through advertisements in a local newspaper and on the departmental website. The main exclusion criteria for HC included a history of major internal or neuropsychiatric diseases, first-degree relatives with dementia, past or current abuse of alcohol or other drugs, intake of psychoactive drugs or anti-inflammatory medication (up to 6 weeks before inclusion) and structural abnormalities on MRI.

AD patients were recruited through the Memory Clinics of the University Hospitals Leuven and the University Hospital Brussels. The main inclusion criteria were: diagnosis of probable AD according to the NINCDS-ADRDA Criteria [17], an MRI scan obtained within the last 12 months consistent with a diagnosis of AD, a positive [¹¹C]-PIB scan (by visual assessment of a trained nuclear medicine physician), a Modified Hachinski Ischemia Scale (MHIS) score of ≤ 4 and a global Clinical Dementia Rating score (CDR) [18] between 1 and 3 (or if the global CDR was 0.5, then the Sum of Boxes was at least 3.5). Recent or routine use of anti-inflammatory medication (6 weeks) was an exclusion criteria in AD patients too.

On the day of the PET scan, all subjects underwent a full clinical examination, blood and urine testing to exclude major disorders and drug abuse. Initially for each group initially 10 subjects were recruited. However, due to HPLC metabolite quantification problems in 2 HC and failure of full PET data acquisition in one anxious AD patient, full quantitative data sets were available in 8 HC and 9 AD patients. Four HC subjects underwent retest scanning within a mean interval of 9 weeks.

The main demographic and clinical/neuropsychological subject characteristics of the included subjects are described in Table 1.

Field Code Changed

Field Code Changed

All participants underwent clinical neurological and neuropsychological evaluation within two weeks of the [¹¹C]-NE40 PET scan. For details, see supplemental table 1.

The study was approved by the local Ethics Committee and written informed consent was obtained from all participants.

Radioligand preparation

[¹¹C]-NE40 was prepared as described previously [19]. Briefly, a helium stream containing [¹¹C]-CH₃I was bubbled through a solution of 200 microgram 2-oxo-7-hydroxy-8-butyloxy-1,2-dihydroquinoline-3-carboxylic acid cyclohexylamide and 2-4 milligram Cs₂CO₃ in 200 microliter dimethylformamide. The chemical and radiochemical purity of [¹¹C]-NE40 was determined using reversed-phase high-performance liquid chromatography (HPLC). Injected radioactivity and specific activity for both subject groups can be found in Table 1. [¹¹C]-PIB was prepared as described previously [20].

Imaging procedure

All subjects were scanned on a HiRez Biograph 16 PET/CT camera (Siemens, Knoxville, TN, USA). All subjects were fasted for 4 hours before PET scanning. Prior to scanning, a radial artery cannula was inserted for blood sampling as well as a venous cannula on the contralateral side for injection.

The subject's head was restrained by a vacuum cushion to reduce movement artifacts during the scan. Following the low dose (11 mAs) CT transmission scan, a bolus of about 220 MBq (see table 1) [¹¹C]-NE40 was injected intravenously and a 90 minute emission acquisition was started in list mode. All frames were Fourier rebinned into 26 frames: 4 frames of 15 seconds, 3 frames of 1 minute, 3 frames of 2 minutes and 16 frames of 5 minutes. Images were reconstructed using an OSEM algorithm (5 iterations, 8 subsets).

Plasma input curves and metabolite analysis

Field Code Changed

Field Code Changed

In all subjects, 2 ml arterial blood samples were withdrawn manually at the following time intervals: every 10 seconds for the first 100 seconds, at 120, 140 and 160 seconds, and at 3, 4, 5, 8, 10, 15, 20, 30, 40, 60, 74 and 90 minutes after injection. Additional 5 ml arterial samples were taken at 5, 10, 20, 40, 60 and 90 minutes to assess the fraction of unchanged [^{11}C]-NE40 in plasma.

All blood samples were centrifuged for 10 minutes at 3000 rotations per minute (relative centrifuge force of 1550 g). For metabolite analysis, 10 μg cold NE40 was added to 1 ml plasma and the mixture was then injected onto the HPLC system as such. The HPLC eluent was collected in two fractions: after 0-15 minutes (metabolite fractions) and 15-20 minutes (parent fraction). A Wallac 1480 gamma counter (PerkinElmer, Waltham, MA, USA) was used to measure the amount of radioactivity of the plasma samples and each HPLC fraction for radiometabolite quantification. The parent fraction of the tracer as a function of time post tracer injection was fitted by a Hill function and then applied to the measured plasma activity resulting in a metabolite corrected arterial input function.

Image analysis

Volume of interest segmentation

All data was segmented and modeled by PMOD (v3.4, Zurich, Switzerland). Interframe motion correction was applied. Individual T1 weighted MRI images were used for VOI delineation (PNEURO tool). PET images were first rigidly coregistered to the corresponding individual volumetric T1 MRI images. The individual T1 MRI images were then nonlinearly coregistered to the standard Montreal Neurological Institute (MNI) space MRI template in PMOD. Subsequently the same was done for the PET images using the same spatial transformation as the registered MR images. Initially, MRI images were segmented into fractions grey matter (GM), white matter (WM) and cerebrospinal fluid (CSF). Next, the

human brain probability maps with 83 VOIs (Hammers template [21]) were applied. VOIs with expected homogeneous CB₂R expression (cortex, subcortical, cerebellum) were united into bigger combination volumes to increase regional specificity. By this means the following 11 combined VOIs were defined : frontal, temporal, parietal and occipital lobes, striatum, thalamus, substantia nigra, cerebellum, insula, cingulate and total grey matter.

Grey matter (GM), white matter (WM) and cerebrospinal fluid (CSF) volume was determined on all datasets by segmentation. Presence of brain atrophy was calculated by determining relative GM volume to the sum of GM, WM and CSF volume.

The dynamic [¹¹C]-NE40 PET activity data (kBq/cc) were spatially coregistered with the subject specific MRI and VOIs were projected onto the PET data to generate time activity curves (TACs).

Kinetic modeling

One tissue (1T2K: K_1, k_2) and two tissue reversible (2T4K: K_1, k_2, k_3, k_4) and irreversible (2T3K: K_1, k_2, k_3) kinetic models with blood volume and arterial metabolite corrected input functions were evaluated to calculate total distribution volume (V_T). Binding potential (BP_{ND}) ~~were~~ ~~as~~ ~~the~~ ~~ratio~~ ~~of~~ ~~k₃/k₄~~ ~~form~~ ~~from~~ ~~the~~ ~~2T4K~~ ~~kinetic~~ ~~model~~. Modeling was performed using weighting factors based on total activity per VOI per frame and frame durations. Various random starting parameter sets were used with each VOI to prevent the solution from being stuck in a local minimum. The best kinetic model was selected based on the Akaike information criterion (AIC) [22]. Spectral analysis was applied to the data to confirm the optimal number of compartments that best fitted the experimental data [23, 24].

Data were calculated for both the global grey matter VOI and to assess regional variability, also for a frontal, temporal, parietal, and cingulate cortex VOI.

Field Code Changed

Formatted: No underline

Formatted: Subscript

Formatted: Subscript

Field Code Changed

Field Code Changed

Field Code Changed

As AD patients may have substantial cortical atrophy which affects the rate of spill-out of PET signal, a partial volume correction (PVC) was applied (Rousset method) within PMOD [25]. The comparison of V_T and BP_{ND} was calculated by means of t-testing from the PVC partial volume corrected VOI group comparison analysis was performed using the data in the above mentioned 11 combined VOIs.

Amyloid deposition was measured in AD patients using [^{11}C]-PIB PET. Forty minutes after a bolus injection of 303.2 ± 23.6 MBq of [^{11}C]-PIB, a 30 minutes scan was started. Image reconstruction (into 6x5 minutes frames, which were checked for motion and added using rigid motion correction) and standardized uptake value ratio (SUVR) analysis were performed as described previously [26]. SUVR was defined by normalization of each VOI to the mean SUV in the cerebellar grey matter. Additionally, for each AD patient, SUVR parametric SUVR amyloid images were coregistered to the subject's MRI and that was spatially normalized to the MNI space as described above. A VOI analysis was performed using the same united VOIs as for the [^{11}C]-NE40 data (see above). A VOI-based correlation analysis was performed between CB2R availability and amyloid deposition.

Statistical analysis

Difference in kinetic parameters between groups was evaluated using Student's t-test. A p value of < 0.05 was defined as statistically significant. Conventional statistics were performed using GraphPad Prism 6 and p-values of VOI comparisons were corrected for multiple comparisons using a Bonferroni correction.

Field Code Changed

Formatted: Subscript

Formatted: Subscript

Field Code Changed

Results

Subject's characteristics and neuropsychological evaluation

Table 1 shows the basic demographic and scan data, as well as the results for the Mini-mental state examination (MMSE) and Beck's depression inventory (BDI). HC were above the age of 40 years, as they served also for other studies as control group, but were significantly younger than the AD patients. However, no correlation between age and CB₂R availability in both subject groups was found for distribution volume V_T and binding potential BP_{ND} values (supplementary Fig. 1). Compared to HC the MMSE score was significantly reduced in AD patients ($p = 0.004$). Two out of 9 AD patients were using cholinesterase inhibitors during the study and one AD patient was using antidepressant medication. Details on the neuropsychological test results are reported in Supplementary Table 1.

Blood input and PET imaging

The mean parent fraction over time for [¹¹C]-NE40 in the HC group is shown in Fig. 1. [¹¹C]-NE40 was metabolized quickly with 50% of parent tracer left 15 minutes post injection (PI) and 20% at the end of the experiment (90 minutes PI) (Fig. 1). Comparison of parent fractions between HC and AD at the different measured metabolisation time points showed no significant differences. Visually, the distribution of [¹¹C]-NE40 brain uptake was uniform all over all grey matter areas, without regions with a remarkable difference in uptake.

Kinetic modeling results

[¹¹C]-NE40 TAC were best fitted by a two tissue reversible model (Fig. 2), since the Akaike information criterion (AIC) indicated that a two tissue reversible model was preferable for 12 subjects (71 %), and a two tissue irreversible model was the best option for 4 patients (24 %). Only in one patient a second compartment was not necessary and an optimal fit was reached

with a one tissue model. Subjects with a better AIC score for an irreversible model nevertheless could be reliably modeled with a reversible model, therefore a two-tissue reversible model was selected as the most appropriate.

The tracer demonstrated slow kinetics with a K_1 of 0.07 ml/min/ml and k_4 of 0.027 1/min in HC (Table 2). The test-retest variability, calculated as $1 - (\text{parameter (day 1)} / \text{parameter (day 2)})$, was 28% and 30% for V_T and BP_{ND} , respectively, in a total grey matter VOI.

CB₂R availability group comparison

The relative GM volume was significantly lower for the AD group (0.50 ± 0.04) compared to HC (0.54 ± 0.02) ($p=0.0078$). Therefore, partial volume correction was applied on all PET datasets.

Kinetic modeling showed ~~that for the total grey matter VOI, that V_T values for all regions were very low (about 1.3 for HC and 1.0 for AD patients), indicating low binding of the tracer throughout the brain in both populations—~~ Furthermore, a significantly lower CB₂R availability ~~was present~~ in AD compared to HC for V_T ~~was seen, which holds for all grouped cortical regions reported in table 2 ($p < 0.001$) ($p = 0.007$) (Table 2), while a trend towards decrease in AD was found—~~ seen for BP_{ND} ~~in total grey matter ($p = 0.08$), for the —and a temporal lobe VOI this was significant lower CB₂R BP_{ND} in temporal lobe ($p = 0.047$). The regional variation in kinetic parameters and the variance of the k-values can also be seen in Table 2. The regional variation is very low, while the variance of the k-parameters is of the order 20-30%, in some cases up to 50% for the AD patients.-~~

~~On a regional basis, Figure 3 shows boxplots of individual regional individual values for the two groups for BP_{ND} and V_T . Overall BP_{ND} and V_T values were low in all regions in both groups.~~ V_T for all VOIs (Fig. 4 and Supplemental Table 2) –was significantly lower in AD patients compared to controls. There was no region with –higher regional binding in AD

Formatted: No underline

Formatted: Subscript

Formatted: Subscript

Formatted: Subscript

Formatted: Subscript

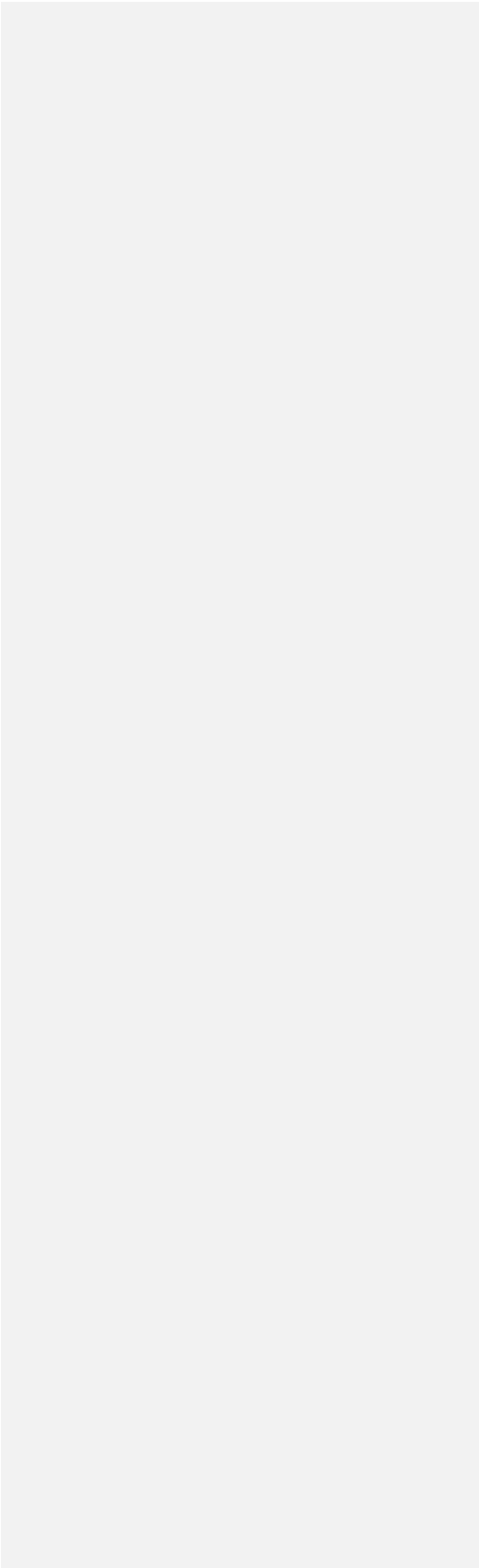
Formatted: Subscript

1
2
3
4
5
6
7
8
9
10
11
12
13
14
15
16
17
18
19
20
21
22
23
24
25
26
27
28
29
30
31
32
33
34
35
36
37
38
39
40
41
42
43
44
45
46
47
48
49
50
51
52
53
54
55
56
57
58
59
60
61
62
63
64
65

patients compared to HC (~~Fig. 5~~). [Figure 5 shows orthogonal images of mean CB2R parametric maps of V_T.](#)

Correlation of CB₂R with amyloid deposition and MMSE in AD patients

We did not observe a regional correlation for homologous VOIs between amyloid deposition and CB₂R availability. No correlation was found between CB₂R availability and neuropsychologic testing results.



Discussion

In this work we have used [¹¹C]-NE40, as a novel radioligand for CB₂R as tentative marker for activated microglia and studied its kinetic modelling in healthy brain and AD patients. We did not find an increased CB₂R availability in AD patients compared to HC as was hypothesized from preclinical and postmortem literature. In contrast, AD patients showed an overall significant decrease of CB₂R availability throughout the brain and this both in cortical and subcortical regions. Moreover no correlation was found between regional amyloid deposition and homologous CB₂R availability in AD patients.

Regarding kinetic modeling of [¹¹C]-NE40, a 2T reversible model provided the best results, and both the BP_{ND} and V_T could be used to quantify CB₂R availability. [¹¹C]-NE40 shows relatively slow kinetics, and with a combination of constants K₁ = 0.07 ml/min/ml and k₃ and k₄ close to 0.02 - 0.03 1/min, the tracer accumulates and dissipates slowly in the bound compartment, enabling appropriate quantification over a 90 minute interval. Time stability of the kinetic parameters was not measured in this study. Test-retest (T-RT) variability for [¹¹C]-NE40 was relatively poor for V_T and BP_{ND} (28 and 30% respectively), but evidently these values are based on low expression levels of activated microglia in the healthy brain and therefore presume low levels of CB₂R. Test-retest values in patients with markedly elevated levels of CB₂R should therefore be considered to address T-RT in pathological circumstances and it is likely that the obtained values in HC should be considered as upper limits.

Previous studies on neuroinflammation in AD (review see [27]), mainly using TSPO markers, have in general shown a pattern of increased neuroinflammation, although some inconsistencies were found. In AD, initial post-mortem findings showed an increase of the number of available binding sites (B_{max}) for [¹¹C]-PK11195 (a TSPO radioligand) in the

Field Code Changed

frontal cortex [28]. In vivo, increased retention of [¹¹C]-PK11195 in patients with mild to moderate AD was found in the entorhinal, temporoparietal and posterior cingulate cortex, corresponding to areas that also show glucose hypometabolism [5]. Kreisl et al. reported a greater TSPO signal using [¹¹C]-PBR28 in AD patients compared to MCI and controls, where the TSPO binding was correlated with disease severity and grey matter loss [29]. However, a recent study by Golla et al. using [¹⁸F] DPA-714 failed to show any increased TSPO binding in AD patients compared to healthy controls [30]. The group of Varrone et al. used [¹⁸F]FEDAA1106 also failed to show an increased binding of TSPO in AD patients [31, 32]. In the latter study, patients had a comparable MMSE as the AD subjects in the present study (25 ± 3). ~~However, as in all these in these studies rs6971 TSPO polymorphism TSPO genotyping was not performed. Although it was discussed whether results with second-generation TSPO tracers, which depends on the TSPO genotype coded by the rs6971 single-nucleotide polymorphism, would be responsible for the lack of TSPO expression difference between controls and the AD population [33], the high variance induced by this grouping of low-, medium and high-binders may which can explain the negative results obtained in these results, our study adds further data that activated microglia may not be present to a significant amount in early AD patients in vivo.~~

However, a number of possible explanations could account for the observed lack of upregulation of CB₂R in AD. Although [¹¹C]-NE40 is a high affinity and selective PET radioligand for CB₂R ($K_{i\text{human}} \text{ CB}_2\text{R} = 9.6\text{nM}$; $K_{i\text{human}} \text{ CB}_1\text{R} = 1000 \text{ nM}$) [19], indicating a hundredfold selectivity over CB₁R, it is known that the CB₁R is one of the most abundantly expressed receptors in the human brain ($B_{\text{max}} > 1 \text{ pmol/mg protein}$) [34]. In contrast, the expression level of CB₂R in brain has been a matter of debate, and to the best of our knowledge, no values for B_{max} of CB₂R in brain tissue has been reported yet. Therefore, regarding sensitivity, the nanomolar affinity of [¹¹C]-NE40 for CB₂R may not be good enough

Field Code Changed

Field Code Changed

Field Code Changed

Field Code Changed

Field Code Changed

Field Code Changed

Field Code Changed

Field Code Changed

Field Code Changed

1
2
3
4
5
6
7
8
9
10
11
12
13
14
15
16
17
18
19
20
21
22
23
24
25
26
27
28
29
30
31
32
33
34
35
36
37
38
39
40
41
42
43
44
45
46
47
48
49
50
51
52
53
54
55
56
57
58
59
60
61
62
63
64
65

1
2
3
4
5
6
7 for detecting neuroinflammation. Also, regarding selectivity, it is therefore conceivable that
8 the measured signal is still influenced by off-target selectivity to CB₁R. However, this cannot
9 explain the observed decrease in AD patients compared to HC, as we recently found that
10 partial-volume corrected CB₁R availability is not altered in AD patients compared to controls
11 [26]. To address this issue in vivo, CB₁R inverse agonist blockade studies could be
12 performed, but these are difficult in view of the retraction of CB₁R inverse agonists from the
13 market [35].

Field Code Changed

Field Code Changed

14
15
16
17
18
19
20 Moreover, several studies have shown that CB₂R in the brain may not only be expressed on
21 activated microglia but also on neuronal cells. Van Sickle et al. reported the presence of CB₂R
22 mRNA and protein in brainstem neurons [36], while Onaivi and Gong studied the distribution
23 of CB₂R in healthy adult rat brain and found low levels of neuronal CB₂R expression in the
24 cerebellum, cortical and subcortical regions [37, 38]. Fernandez-Ruiz et al. reported
25 expression of CB₂R in microglia, astrocytes and neuronal subpopulations, using a variety of
26 neurodegenerative disease models [39]. A recent study by Horti et al. in an AD mouse model,
27 showed CB₂R immunoreactivity in activated microglia but also in neuronal cells [8]. The
28 authors found an enhanced CB₂R signal that was attributed to microglial activation instead of
29 neuronal cell loss. It may therefore be possible that the CB₂R PET signal in this study does
30 not only derive from microglial CB₂R but also from neuronal CB₂R expression and the
31 decreased CB₂R availability in AD patients could be explained by a loss of neuronal cells
32 expressing CB₂R that is incompletely compensated by atrophy correction.

Field Code Changed

Field Code Changed

Field Code Changed

Field Code Changed

Field Code Changed

33
34
35
36
37
38
39
40
41
42
43
44
45 A limitation of our study is that the healthy controls who were included for other pathological
46 studies too, were significantly younger than AD patients. However in our sample, no
47 correlation was found between age and [¹¹C]-NE40 uptake in both HC and AD subgroups
48 (Supplementary Fig. 1), therefore it seems unlikely that our results were influenced by this
49 confounder.
50
51
52
53
54
55
56
57
58
59
60
61
62
63
64
65

In conclusion, using appropriately quantifiable [¹¹C]-NE40 PET, we found a lack of upregulation of CB₂R in AD brain *in vivo* compared to healthy controls without any correlation to regional amyloid deposition. In contrast, CB₂R availability was significantly decreased in AD patients which may indicate a relative loss of neuronal expression rather than absence of microglial expression, therefore making the CB₂R target less promising as biomarker for neuroinflammation in AD.

Compliance with Ethical Standards

The authors declare that they have no conflict of interest.

All procedures performed in this study were in accordance with the ethical standards of the institutional and/or national research committee and with the 1964 Helsinki declaration and its later amendments or comparable ethical standards.

Informed consent was obtained from all individual participants included in the study.

Reference list

1. Jack CR, Jr., Knopman DS, Jagust WJ, Petersen RC, Weiner MW, Aisen PS, et al. Tracking pathophysiological processes in Alzheimer's disease: an updated hypothetical model of dynamic biomarkers. *Lancet neurology*. 2013;12:207-16.
2. Tansey MG, Goldberg MS. Neuroinflammation in Parkinson's disease: its role in neuronal death and implications for therapeutic intervention. *Neurobiology of disease*. 2010;37:510-8.
3. Heneka MT, Carson MJ, El Khoury J, Landreth GE, Brosseron F, Feinstein DL, et al. Neuroinflammation in Alzheimer's disease. *Lancet neurology*. 2015;14:388-405. doi:10.1016/S1474-4422(15)70016-5.
4. Ory D, Celen S, Verbruggen A, Bormans G. PET radioligands for in vivo visualization of neuroinflammation. *Current pharmaceutical design*. 2014;20:5897-913.
5. Cagnin A, Brooks DJ, Kennedy AM, Gunn RN, Myers R, Turkheimer FE, et al. In-vivo measurement of activated microglia in dementia. *Lancet*. 2001;358:461-7.
6. Schuitemaker A, Kropholler MA, Boellaard R, van der Flier WM, Kloet RW, van der Doef TF, et al. Microglial activation in Alzheimer's disease: an (R)-[(1)(1)C]PK11195 positron emission tomography study. *Neurobiology of aging*. 2013;34:128-36.
7. Carrier EJ, Patel S, Hillard CJ. Endocannabinoids in neuroimmunology and stress. *CurrDrug TargetsCNSNeurolDisord*. 2005;4:657-65.
8. Savonenko AV, Melnikova T, Wang Y, Ravert H, Gao Y, Koppel J, et al. Cannabinoid CB2 Receptors in a Mouse Model of Abeta Amyloidosis: Immunohistochemical Analysis and Suitability as a PET Biomarker of Neuroinflammation. *PloS one*. 2015;10:e0129618.

- 1
2
3
4
5
6
7 9. Benito C, Nunez E, Tolon RM, Carrier EJ, Rabano A, Hillard CJ, et al. Cannabinoid
8
9 CB2 receptors and fatty acid amide hydrolase are selectively overexpressed in neuritic
10
11 plaque-associated glia in Alzheimer's disease brains. *J Neurosci.* 2003;23:11136-41.
- 12
13 10. Palazuelos J, Aguado T, Pazos MR, Julien B, Carrasco C, Resel E, et al. Microglial
14
15 CB2 cannabinoid receptors are neuroprotective in Huntington's disease excitotoxicity. *Brain.*
16
17 2009;132:3152-64.
- 18
19 11. Price DA, Martinez AA, Seillier A, Koek W, Acosta Y, Fernandez E, et al.
20
21 WIN55,212-2, a cannabinoid receptor agonist, protects against nigrostriatal cell loss in the 1-
22
23 methyl-4-phenyl-1,2,3,6-tetrahydropyridine mouse model of Parkinson's disease. *Eur J*
24
25 *Neurosci.* 2009;29:2177-86.
- 26
27 12. Slavik R, Herde AM, Bieri D, Weber M, Schibli R, Kramer SD, et al. Synthesis,
28
29 radiolabeling and evaluation of novel 4-oxo-quinoline derivatives as PET tracers for imaging
30
31 cannabinoid type 2 receptor. *European journal of medicinal chemistry.* 2015;92:554-64.
- 32
33 13. Hortala L, Arnaud J, Roux P, Oustric D, Boulu L, Oury-Donat F, et al. Synthesis and
34
35 preliminary evaluation of a new fluorine-18 labelled triazine derivative for PET imaging of
36
37 cannabinoid CB2 receptor. *Bioorganic & medicinal chemistry letters.* 2014;24:283-7.
- 38
39 14. Teodoro R, Moldovan RP, Lueg C, Gunther R, Donat CK, Ludwig FA, et al.
40
41 Radiofluorination and biological evaluation of N-aryl-oxadiazolyl-propionamides as potential
42
43 radioligands for PET imaging of cannabinoid CB2 receptors. *Organic and medicinal*
44
45 *chemistry letters.* 2013;3:11.
- 46
47 15. Ahmad R, Koole M, Evens N, Serdons K, Verbruggen A, Bormans G, et al. Whole-
48
49 Body Biodistribution and Radiation Dosimetry of the Cannabinoid Type 2 Receptor Ligand
50
51 [C]-NE40 in Healthy Subjects. *Molecular imaging and biology : MIB : the official publication*
52
53 *of the Academy of Molecular Imaging.* 2013.
- 54
55
56
57
58
59
60
61
62
63
64
65

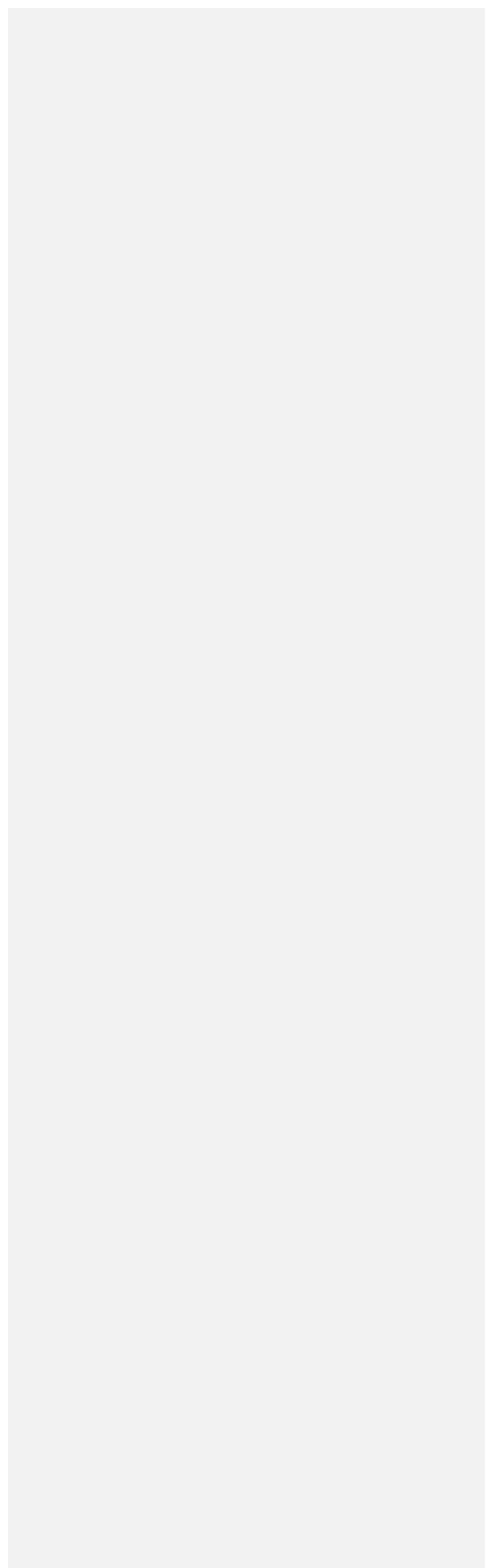
16. Evens N, Vandeputte C, Coolen C, Janssen P, Sciot R, Baekelandt V, et al. Preclinical evaluation of [¹¹C]NE40, a type 2 cannabinoid receptor PET tracer. *NuclMedBiol.* 2012;39:389-99.
17. Dubois B, Feldman HH, Jacova C, DeKosky ST, Barberger-Gateau P, Cummings J, et al. Research criteria for the diagnosis of Alzheimer's disease: revising the NINCDS-ADRDA criteria. *Lancet Neurol.* 2007;6:734-46.
18. Morris JC. The Clinical Dementia Rating (CDR): current version and scoring rules. *Neurology.* 1993;43:2412-4.
19. Evens N, Muccioli GG, Houbrechts N, Lambert DM, Verbruggen AM, Van LK, et al. Synthesis and biological evaluation of carbon-11- and fluorine-18-labeled 2-oxoquinoline derivatives for type 2 cannabinoid receptor positron emission tomography imaging. *Nucl Med Biol.* 2009;36:455-65.
20. Burns HD, Van Laere K, Sanabria-Bohorquez S, Hamill TG, Bormans G, Eng WS, et al. [¹⁸F]MK-9470, a positron emission tomography (PET) tracer for in vivo human PET brain imaging of the cannabinoid-1 receptor. *ProcNatlAcadSciUSA.* 2007;104:9800-5.
21. Hammers A, Allom R, Koepp MJ, Free SL, Myers R, Lemieux L, et al. Three-dimensional maximum probability atlas of the human brain, with particular reference to the temporal lobe. *Human brain mapping.* 2003;19:224-47.
22. Akaike. A new look at the statistical model identification. *IEEE transactions on automatic control.* 1974;ac-19:716-23.
23. Gunn RN, Gunn SR, Turkheimer FE, Aston JA, Cunningham VJ. Positron emission tomography compartmental models: a basis pursuit strategy for kinetic modeling. *Journal of cerebral blood flow and metabolism : official journal of the International Society of Cerebral Blood Flow and Metabolism.* 2002;22:1425-39.

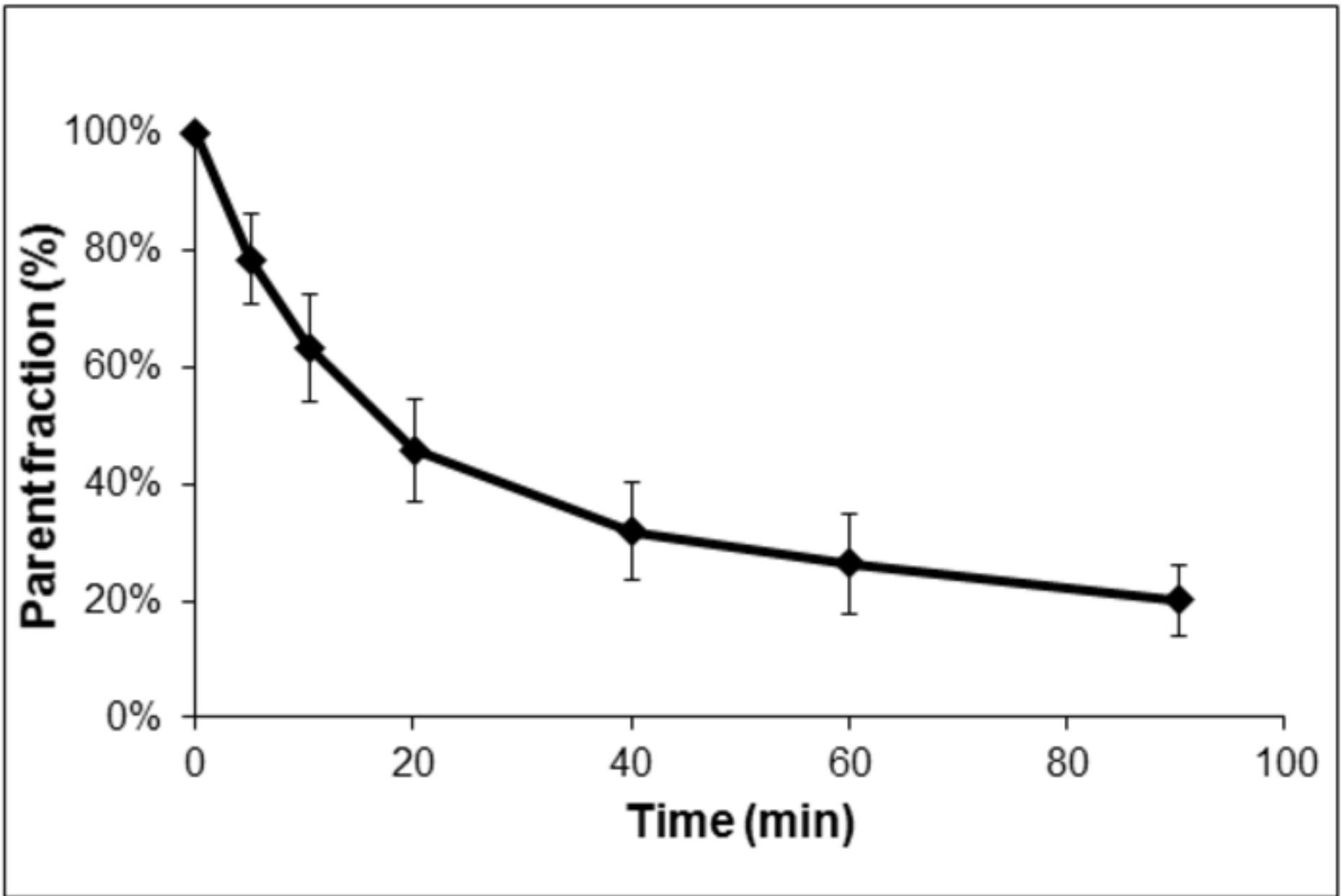
- 1
2
3
4
5
6
7
8
9
10
11
12
13
14
15
16
17
18
19
20
21
22
23
24
25
26
27
28
29
30
31
32
33
34
35
36
37
38
39
40
41
42
43
44
45
46
47
48
49
50
51
52
53
54
55
56
57
58
59
60
61
62
63
64
65
24. Cunningham VJ, Jones T. Spectral analysis of dynamic PET studies. *Journal of cerebral blood flow and metabolism : official journal of the International Society of Cerebral Blood Flow and Metabolism*. 1993;13:15-23.
 25. Rousset OG, Ma Y, Evans AC. Correction for partial volume effects in PET: principle and validation. *J Nucl Med*. 1998;39:904-11.
 26. Ahmad R, Goffin K, Van den Stock J, De Winter FL, Cleeren E, Bormans G, et al. In vivo type 1 cannabinoid receptor availability in Alzheimer's disease. *European neuropsychopharmacology : the journal of the European College of Neuropsychopharmacology*. 2013.
 27. Janssen B, Vugts DJ, Funke U, Molenaar GT, Kruijer PS, van Berckel BN, et al. Imaging of neuroinflammation in Alzheimer's disease, multiple sclerosis and stroke: Recent developments in positron emission tomography. *Biochimica et biophysica acta*. 2015. doi:10.1016/j.bbadis.2015.11.011.
 28. Veneti S, Lopresti BJ, Wang G, Hamilton RL, Mathis CA, Klunk WE, et al. PK11195 labels activated microglia in Alzheimer's disease and in vivo in a mouse model using PET. *Neurobiology of aging*. 2009;30:1217-26.
 29. Kreisl WC, Lyoo CH, McGwier M, Snow J, Jenko KJ, Kimura N, et al. In vivo radioligand binding to translocator protein correlates with severity of Alzheimer's disease. *Brain*. 2013;136:2228-38.
 30. Golla SS, Boellaard R, Oikonen V, Hoffmann A, van Berckel BN, Windhorst AD, et al. Quantification of [18F]DPA-714 binding in the human brain: initial studies in healthy controls and Alzheimer's disease patients. *Journal of cerebral blood flow and metabolism : official journal of the International Society of Cerebral Blood Flow and Metabolism*. 2015;35:766-72. doi:10.1038/jcbfm.2014.261.

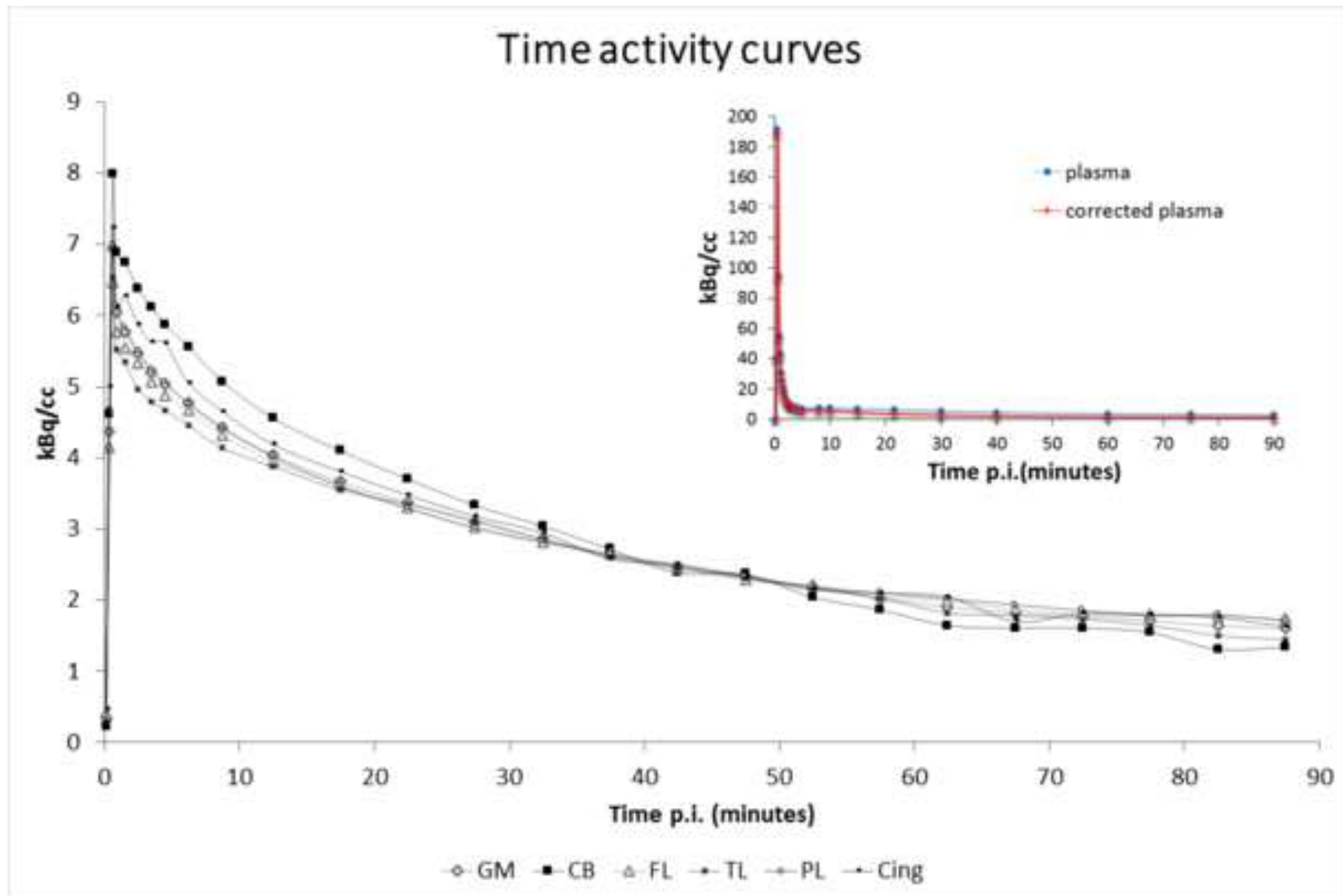
- 1
2
3
4
5
6
7 31. Varrone A, Mattsson P, Forsberg A, Takano A, Nag S, Gulyas B, et al. In vivo
8 imaging of the 18-kDa translocator protein (TSPO) with [¹⁸F]FEDAA1106 and PET does not
9 show increased binding in Alzheimer's disease patients. *European journal of nuclear medicine*
10 *and molecular imaging*. 2013;40:921-31.
11
12 32. Stefaniak J, O'Brien J. Imaging of neuroinflammation in dementia: a review. *Journal*
13 *of neurology, neurosurgery, and psychiatry*. 2015.
14
15 33. Fan Z, Harold D, Pasqualetti G, Williams J, Brooks DJ, Edison P. Can Studies of
16 Neuroinflammation in a TSPO Genetic Subgroup (HAB or MAB) Be Applied to the Entire
17 AD Cohort? *J Nucl Med*. 2015;56:707-13.
18
19 34. Howlett AC, Barth F, Bonner TI, Cabral G, Casellas P, Devane WA, et al.
20 International Union of Pharmacology. XXVII. Classification of cannabinoid receptors.
21 *PharmacolRev*. 2002;54:161-202.
22
23 35. Christensen R, Kristensen PK, Bartels EM, Bliddal H, Astrup A. Efficacy and safety
24 of the weight-loss drug rimonabant: a meta-analysis of randomised trials. *Lancet*.
25 2007;370:1706-13.
26
27 36. Van Sickle MD, Duncan M, Kingsley PJ, Mouihate A, Urbani P, Mackie K, et al.
28 Identification and functional characterization of brainstem cannabinoid CB2 receptors.
29 *Science*. 2005;310:329-32.
30
31 37. Gong JP, Onaivi ES, Ishiguro H, Liu QR, Tagliaferro PA, Brusco A, et al.
32 Cannabinoid CB2 receptors: immunohistochemical localization in rat brain. *Brain research*.
33 2006;1071:10-23.
34
35 38. Onaivi ES, Ishiguro H, Gong JP, Patel S, Perchuk A, Meozzi PA, et al. Discovery of
36 the presence and functional expression of cannabinoid CB2 receptors in brain.
37 *AnnNYAcadSci*. 2006;1074:514-36.
38
39
40
41
42
43
44
45
46
47
48
49
50
51
52
53
54
55
56
57
58
59
60
61
62
63
64
65

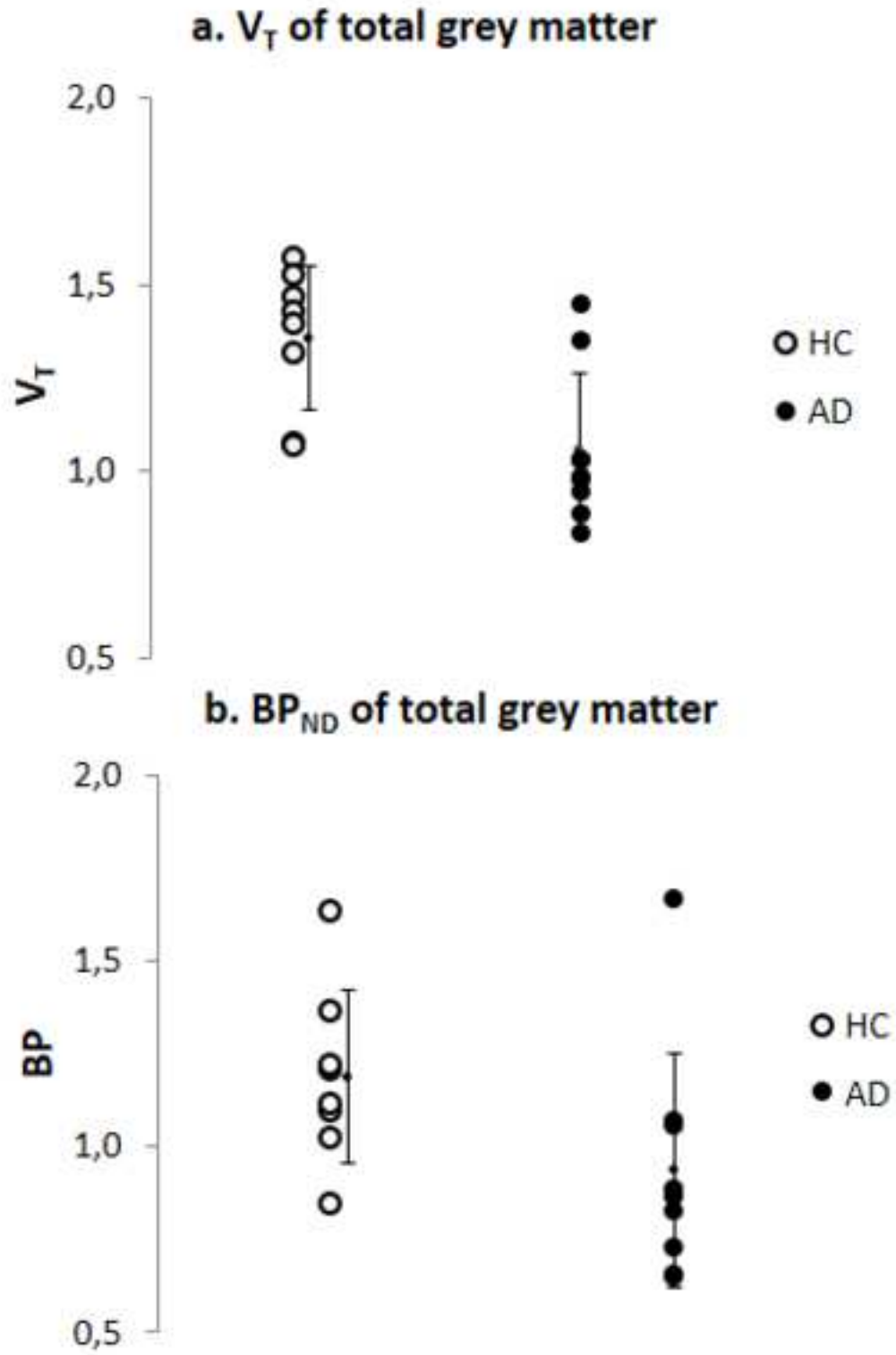
1
2
3
4
5
6
7
8
9
10
11
12
13
14
15
16
17
18
19
20
21
22
23
24
25
26
27
28
29
30
31
32
33
34
35
36
37
38
39
40
41
42
43
44
45
46
47
48
49
50
51
52
53
54
55
56
57
58
59
60
61
62
63
64
65

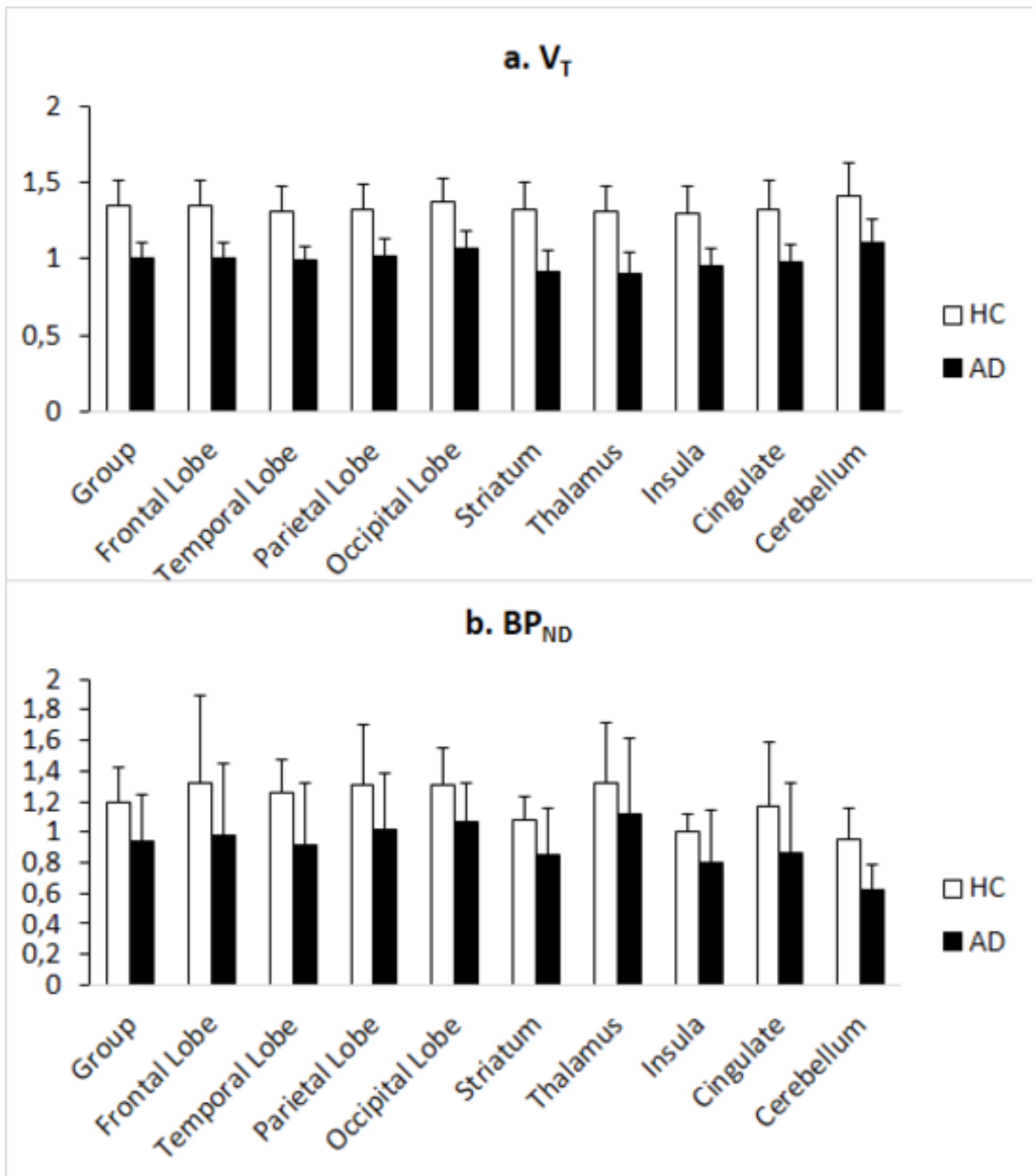
39. Fernandez-Ruiz J, Romero J, Velasco G, Tolon RM, Ramos JA, Guzman M.
Cannabinoid CB2 receptor: a new target for controlling neural cell survival? Trends
PharmacolSci. 2007;28:39-45.

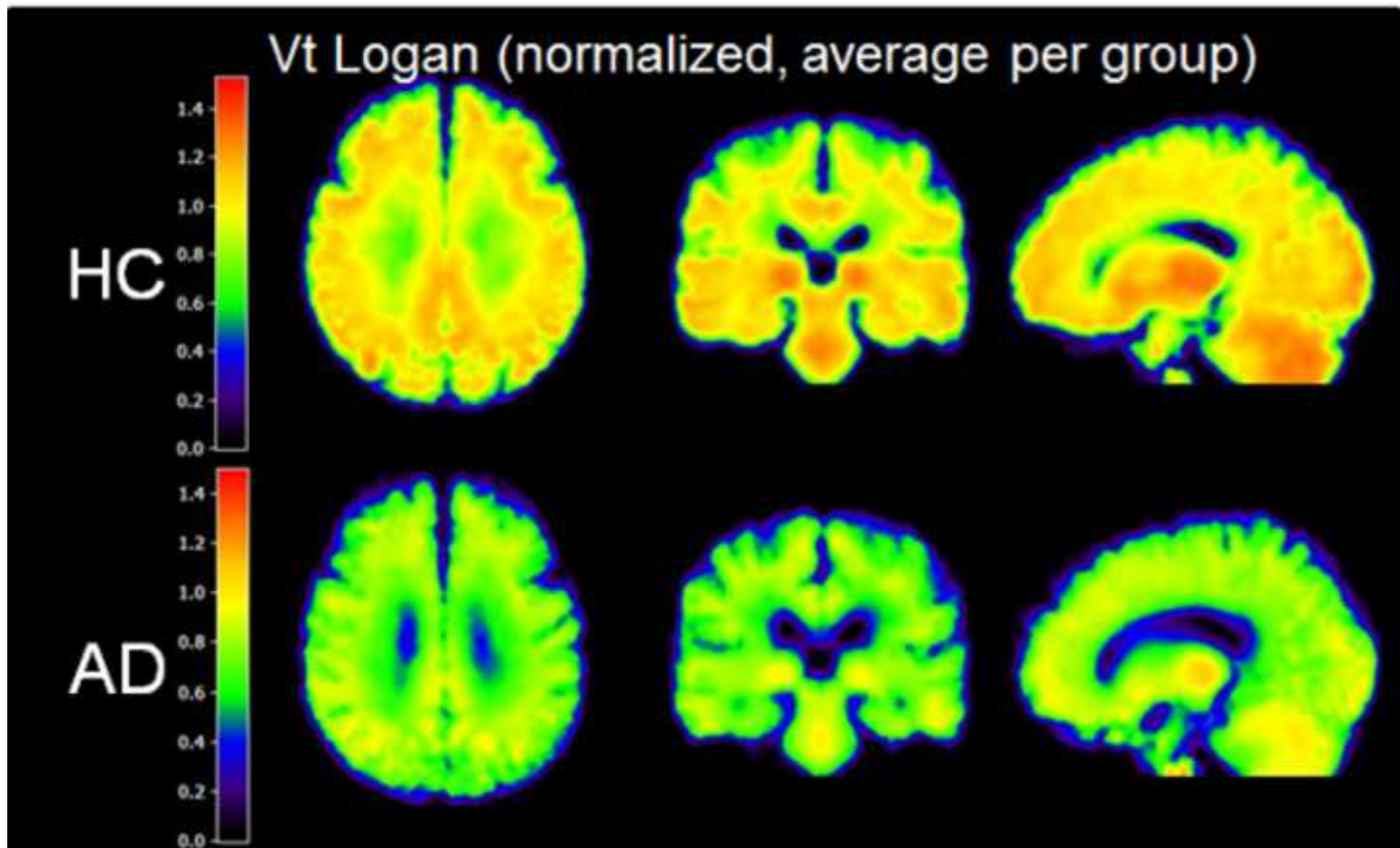












Legend figures

Fig. 1 Parent fraction in plasma as a function of time. Error bars indicate one standard deviation.

Fig. 2 Time activity curves in target regions of a representative AD patients (GM total grey matter, CB cerebellum, FL frontal lobe, TL temporal lobe, and PL ~~parietal~~ parietal lobe). Insert shows Representative [¹¹C]-NE40 time activity curve fitted with one (1T) and two tissue (2T) models. ~~the total and metabolite-corrected time~~ plasma activity curve for the same AD patient.

Fig. 3 Individual variability in (a) distribution volume (V_T) and (b) binding potential (BP_{ND}) for all grey matter VOI voxels. In black next to the data points, the error bar indicate one standard deviation from the average per group. HC = healthy controls; AD = Alzheimer's disease patients

Fig. 4 a: Distribution volume V_T for different volumes of interest. b: Binding potential BP_{ND} calculated from a two tissue reversible model. HC = healthy control; AD = Alzheimer's disease patients

Fig. 5 ~~Transaxial, coronal and sagittal M_{mean} CB₂-receptor~~ CB_2R binding parametric maps per group calculated from distribution volume by Logan graphic analysis after a bolus injection of [¹¹C]-NE40. Images were first smoothed with an isotropic Gaussian kernel with a full width at half maximum (FWHM) of 8 mm. HC = healthy controls; AD = Alzheimer's disease patients

Formatted: Space After: 0 pt, Don't adjust space between Latin and Asian text, Don't adjust space between Asian text and numbers

Formatted: Font: (Default) Times New Roman, 12 pt, English (United States)

Formatted: Font: (Default) Times New Roman, 12 pt, English (United States)

Commented [KL1]: titel verwijderen van PDF..

Commented [KL2]: the x-axis line is too light grey and has no ticks : make black and add ticks. The symbols should be in the figure, not in the bottom for JNM.

Formatted: Space After: 0 pt, Line spacing: single, Don't adjust space between Latin and Asian text, Don't adjust space between Asian text and numbers

Formatted: Subscript

Formatted: Subscript

Formatted: Subscript

Formatted: Subscript

Formatted: Subscript

Table 1 Characteristics of the healthy controls and AD patients ~~included in this study~~.

	HC	HC retest	AD
Gender (M/F)	4/4	2/2	7/2
Age (years)	54.0 ± 10.0	59.4 ± 6.9	73.4 ± 8.7 *
Disease duration	NA	NA	2.3 ± 1.3
MMSE score (/30)	29.6 ± 0.8	29.3 ± 0.9	25.0 ± 3.2 *
BDI	5.0 ± 3.4	5.5 ± 4.0	6.4 ± 3.2
Injected activity [¹¹ C]-NE40 (MBq)	209.0 ± 47.88	219.0 ± 63.94	245.3 ± 37.1
Injected activity [¹¹ C]-PIB (MBq)	NA	NA	303.2 ± 23.6
Specific radioactivity <u>at EOS of [¹¹C]-NE40</u> (GBq/μmol)	327.3 ± 1298.7	218.5 ± 105.5	2154.7 ± 1121.7

HC = Healthy controls; AD = Alzheimer's disease patients; M= male; F = female; MMSE = Mini-mental state examination; BDI = Beck depression inventory; NA = not applicable; EOS = end of synthesis

Data are reported as mean ± standard deviation

* p < 0.05 compared to HC

Formatted: Not Superscript/ Subscript

graphic analysis. BP = binding potential. GM = grey matter (GM). FL = frontal lobe (FL).

TL = temporal lobe (TL). PL = parietal lobe (PL). CG = cingulum (CL).

Formatted: Not Superscript/ Subscript

Formatted: Not Superscript/ Subscript

Formatted: Not Superscript/ Subscript

Formatted: Not Superscript/ Subscript

Formatted: Not Superscript/ Subscript

Formatted: English (United States)

Formatted: Line spacing: Double